PHYSICAL REVIEW FLUIDS **2**, 124204 (2017)

Isotropic stochastic rotation dynamics

Sebastian Mühlbauer,* Severin Strobl, and Thorsten Pöschel
Institute for Multiscale Simulation, Friedrich-Alexander-Universität Erlangen-Nürnberg, Nägelsbachstraße 49b, 91052 Erlangen, Germany
(Received 29 May 2017; published 22 December 2017)

Stochastic rotation dynamics (SRD) is a widely used method for the mesoscopic modeling of complex fluids, such as colloidal suspensions or multiphase flows. In this method, however, the underlying Cartesian grid defining the coarse-grained interaction volumes induces anisotropy. We propose an isotropic, lattice-free variant of stochastic rotation dynamics, termed iSRD. Instead of Cartesian grid cells, we employ randomly distributed spherical interaction volumes. This eliminates the requirement of a grid shift, which is essential in standard SRD to maintain Galilean invariance. We derive analytical expressions for the viscosity and the diffusion coefficient in relation to the model parameters, which show excellent agreement with the results obtained in iSRD simulations. The proposed algorithm is particularly suitable to model systems bound by walls of complex shape, where the domain cannot be meshed uniformly. The presented approach is not limited to SRD but is applicable to any other mesoscopic method, where particles interact within certain coarse-grained volumes.

DOI: 10.1103/PhysRevFluids.2.124204

I. INTRODUCTION

During recent years, particle-based fluid simulation methods have been well established as an alternative to continuum methods. They have important advantages, especially in situations where the continuum assumption does not hold, but also for complex fluids, such as colloidal suspensions, or multiphase flows [1–5]. With molecular dynamics, for example, complex fluids can be simulated on the molecular level including the actual microscopic interaction laws [6]. In contrast, the particles employed in direct simulation Monte Carlo (DSMC) [7] do not represent physical particles, but rather probability quanta, composing the velocity distribution function. In DSMC, the particle trajectories are not computed deterministically, as in molecular dynamics. Instead, binary collisions are performed to model the transport of momentum and eventually solve the nonlinear Boltzmann equation [8]. Thus, unlike computational fluid dynamics (CFD), based on the numerical solution of hydrodynamic equations, DSMC does not rely on relations between the hydrodynamic fields and is also reliable in cases where the hydrodynamic description of the system is problematic, for instance, in the presence of shocks [9]. Further important fields of application are flows at moderate to high Knudsen number, such as rarefied gases [10], flows in the vicinity of boundaries [11], or flows in microfluidic devices [12], where the mean free path does not fulfill the condition of being much smaller than the system dimensions. In most cases, DSMC consumes significantly larger computational resources than field-based CFD. In return, it has a wider range of validity than CDF, since it relies exclusively on the validity of the Boltzmann description. Moreover, there are also applications for which DSMC is computationally efficient, e.g., rarefied gas flows with a large mean free path, and rather few particle collisions, since the computational cost of DSMC is proportional to the particle collision rate.

For application to denser gases, however, stochastic rotation dynamics (SRD), developed by Malevanets and Kapral [13], is more efficient, compromising between DSMC and CFD: Instead of numerous binary collision, one so-called multiparticle collision is performed to exchange momentum

*Corresponding author: sebastian.muehlbauer@fau.de

between all particles within certain coarse-graining volumes, which usually are the cells of a Cartesian grid spanning the simulation volume. The size as well as the shape of the coarse-graining volumes has significant influence on the transport coefficients. Therefore, a grid composed of cubic cells is used for the majority of applications. In order to model complicated domains, an additional surface grid, describing the boundaries, has to be embedded into the regular simulation grid. It was shown that in its basic form, SRD does not preserve Galilean invariance, which can be corrected by a random *grid shift*, that is, the simulation grid has to be shifted randomly before each collision step [14]. The grid shift assures Galilean invariance; however, it does not correct the anisotropy caused by the underlying cubic grid [15]. Ihle *et al.* [15] conjectured that additional random grid rotations would restore isotropy in SRD.

For the case of DSMC, which suffers from similar problems, in order to achieve isotropy, Donev *et al.* [16] suggest a grid-free version, termed isotropic DSMC (iDSMC). While in standard DSMC only particles from the same grid cell are allowed to collide, in iDSMC random particle pairs are chosen to transfer momentum, if they are not further apart than a given distance, disregarding their cell affiliation. This procedure leads to an isotropic interaction between the quasiparticles [16,17].

Following a similar idea, we propose a grid-free, truly Lagrangian version of SRD which we call *isotropic stochastic rotation dynamics* (iSRD).

We will first provide a short review of SRD and the corresponding relations for the transport coefficients. Subsequently, we will describe our approach to eliminate the influence of the spatial discretization and derive analytical expressions for the viscosity and the diffusion coefficient in this case. Finally, we compare these expressions with measurements of the transport coefficients obtained from simulations.

II. STOCHASTIC ROTATION DYNAMICS

SRD is a Lagrangian approach, where the fluid is represented by particles. Each time step of the simulation, Δt, comprises a streaming and a collision step. The streaming step propagates the particles according to their current velocity,

$$\vec{r}_i(t + \Delta t) = \vec{r}_i(t) + \Delta t\, \vec{v}_i(t)\,, \tag{1}$$

where $\vec{r}_i$ and $\vec{v}_i$ denote the position and velocity of particle i, respectively. The collision step randomly rotates the fluctuating contribution to the particles' velocities, which is related to the temperature of the fluid, according to the collision rule

$$\vec{v}_i(t + \Delta t) = \vec{u}(t)|_i + \hat{R} \cdot [\vec{v}_i(t) - \vec{u}(t)|_i]\,, \tag{2}$$

where $\vec{u}(t)$ is the macroscopic flow velocity field and $\vec{u}(t)|_i$ is the value of the field at the location of particle i. In SRD, the field $\vec{u}$ is obtained by coarse graining the velocities of all particles of the system, using a Cartesian grid spanning the simulation domain. Thus, the flow velocity corresponding to the ith particle is estimated as the mean velocity of all particles residing in the same grid cell, C, as $\vec{u}(t)|_i \equiv \langle \vec{v} \rangle^C$, and the particle's thermal velocity is $[\vec{v}_i(t) - \langle \vec{v} \rangle^C]$. In three-dimensional simulations, the rotation matrix, $\hat{R}$, represents a rotation by a constant rotation angle, α, where the rotation axis is randomly chosen in each collision step for each grid cell [1,13].

As an example and for later reference, in Fig. 1 we present the flow profile for plane Poiseuille flow with simple bounce-back boundary conditions [18] at the walls and periodic boundaries in the other two spatial directions. The SRD implementation used is built on the framework developed by Strobl [19]. If not specified otherwise, here and in the following we use dimensionless parameters, that is, the cell width $a = 1$, time step $\Delta t = 0.1$, thermal velocity $\sqrt{k\,T/m} = 1$, and the rotation angle $\alpha = \pi/2$. The number of particles is chosen such that on average $M = 10$ particles reside in each grid cell. The flow is driven by an external acceleration of 5×10^{-3}. Temperature is kept constant by means of the cell-level thermostat which was developed by Hecht *et al.* [20,21] based on Refs. [22,23]. To obtain the flow profile shown in Fig. 1, we average the particle velocities within slices parallel to the channel walls, considering two different slice widths. For the symbols (○), the

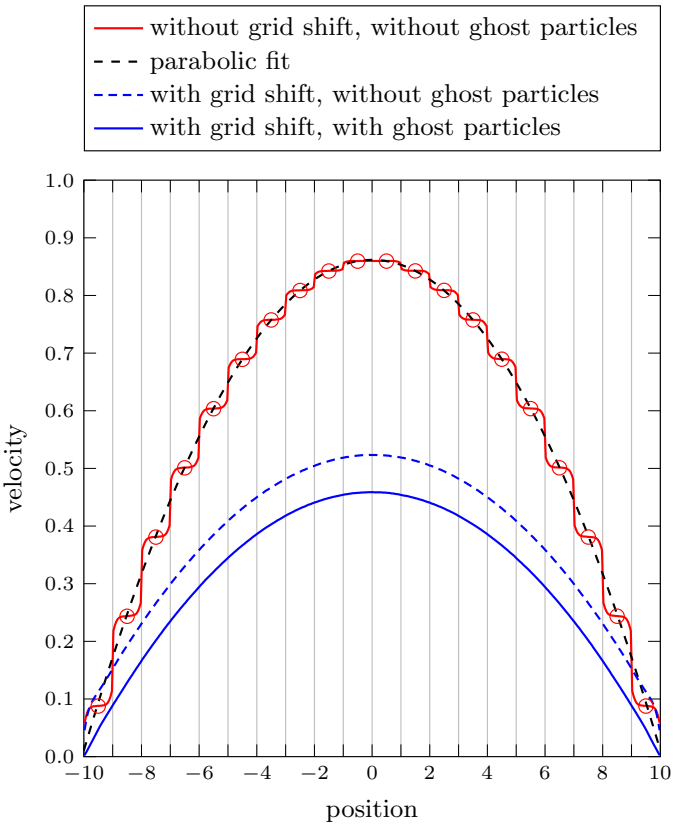

FIG. 1. The upper curves correspond to plane Poiseuille flow simulated using SRD without grid shift. The discretization of the channel, which is 20 cells wide, is shown by the vertical thin lines. The particle velocities are averaged within slices oriented parallel to the channel walls. The symbols (○) show the average particle velocity within slices having width a. The upper dashed line is a parabola fitted to this averaged velocity profile in the interval $[-5,5]$, i.e., distant from the walls. The red solid line represents the detailed flow profile, obtained by averaging within slices of width $a/20$. The two lower curves show the results for SRD with grid shift, using the same parameters as before. To reduce velocity slip at the walls, for the solid blue line, ghost particles (see Sec. V E) were used in addition to the grid shift.

slice width is chosen to be equal to the cell width, a. These cell averaged velocities agree very well with the fitted parabola drawn as a dashed line. Considering, however, the solid line representing the finer resolved flow profile, which is obtained by averaging within slices having a width of $a/20$, we perceive distinct steps, connecting the plateaus within the simulation cells. This effect reveals a violation of the molecular chaos assumption: In case the mean free path is small compared to the cell width, many particles remain in one grid cell for several time steps, colliding with each other repeatedly and, thus, correlating the velocities of the particles in the same cell. To reduce precollisional correlations and to make SRD Galilean invariant, the so-called grid shift [1,14] can be applied: Before each collision step the simulation grid is shifted by a random vector $\vec{s} = [s_x, s_y, s_z]$, with $s_x, s_y, s_z \in [-a/2, a/2]$. This procedure is sensible, only as long as the simulation domain is discretized using a regular cubic grid. For the setup from Fig. 1, the grid shift enhances the transport of momentum across the channel, i.e., the shear viscosity [24]. Activating the grid shift leads to smooth velocity profiles: The solid and dashed blue lines represent the corresponding simulation results with and without ghost particles, as introduced in Sec. V E, respectively.

III. TRANSPORT COEFFICIENTS IN SRD

As pointed out in Ref. [1], different approaches have been applied to characterize the SRD fluid. While in some works [15,24–27] the transport coefficients are investigated based on equilibrium calculations, other authors consider the system's response to imposed nonequilibrium conditions [28,29]. Both approaches lead to identical results for the transport coefficients. The viscosity of a fluid simulated with SRD is known to have two contributions, which are denoted as the *kinetic* and the *collisional* parts [30]. Under the assumption of molecular chaos, Kikuchi *et al.* [28] derive analytical expressions for these two contributions. Considering stationary Couette flow with the flow profile $\vec{u}(y) = [\dot{\gamma}\, y, 0, 0]$, where the shear rate, $\dot{\gamma} \equiv \partial u_x(y)/\partial y$, is constant, Kikuchi *et al.* find for the kinetic contribution to the viscosity in the three-dimensional case

$$\nu_{\mathrm{SRD}}^{\mathrm{kin}} = \frac{k_B\, T}{m} \Delta t \left(\frac{1}{2} + \frac{f}{1-f} \right), \tag{3}$$

where k_B, T, and m denote the Boltzmann constant, the temperature, and the particle mass, respectively. The term

$$f(\alpha, n) = 1 - \left(\frac{n-1}{n} \right) \frac{2}{5} (2 - \cos\alpha - \cos 2\alpha) \tag{4}$$

describes the relative change in the correlation $\langle v_x\, v_y \rangle$ due to the collision operator from Eq. (2) in case exactly n particles are contained in the considered grid cell,

$$\langle v_x(t + \Delta t)\, v_y(t + \Delta t) \rangle = f(\alpha, n)\, \langle v_x(t)\, v_y(t) \rangle. \tag{5}$$

However, the number of particles, n, contained in the collision cells is not constant but Poisson distributed. Averaging over $n \in \{1, 2, \ldots, \infty\}$ yields

$$f(\alpha, M) = 1 - \frac{M - 1 + e^{-M}}{M} \frac{2}{5} (2 - \cos\alpha - \cos 2\alpha) \tag{6}$$

and

$$\langle v_x(t + \Delta t)\, v_y(t + \Delta t) \rangle = f(\alpha, M)\, \langle v_x(t)\, v_y(t) \rangle, \tag{7}$$

with M being the average number of particles per cell. An analogous procedure leads to an analytical expression for the diffusion coefficient, having no collisional contribution [1],

$$D_{\mathrm{SRD}} = \frac{k_B\, T}{m} \Delta t \left(\frac{1}{2} + \frac{g}{1-g} \right), \tag{8}$$

where

$$g(\alpha, M) = 1 - \frac{M - 1 + e^{-M}}{M} \frac{2}{3} (1 - \cos\alpha). \tag{9}$$

In order to obtain the collisional part of the viscosity, Kikuchi *et al.* [28] compute the momentum exchange along the direction of the velocity gradient due to the collision step for the considered Couette flow and obtain

$$\nu_{\mathrm{SRD}}^{\mathrm{coll}} = \frac{a^2}{18\, \Delta t} \frac{M - 1 + e^{-M}}{M} (1 - \cos\alpha). \tag{10}$$

For the derivation of Eq. (10), the flow profile is required to be smooth, which can be accomplished by the use of a grid shift, as shown in Fig. 1. The results for the kinetic part of the viscosity, Eq. (3) together with Eq. (6), as well as for the collisional contribution, Eq. (10), match the corresponding simulation results [28].

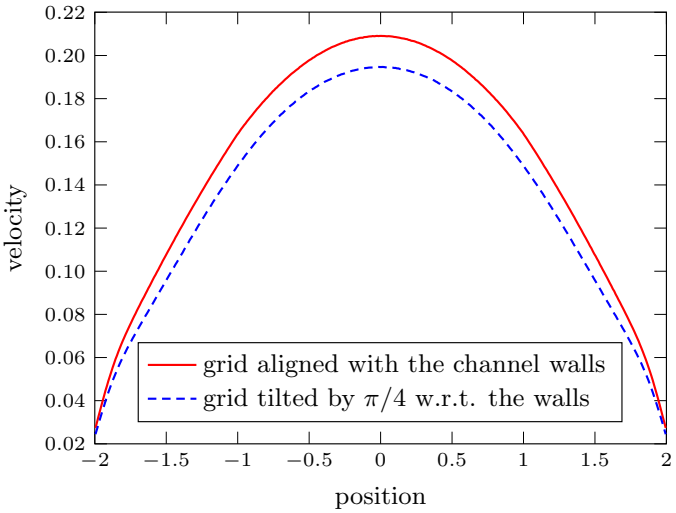

FIG. 2. Plane Poiseuille flow simulated using SRD with grid shift and two different grid orientations. The channel walls are modeled following the approach described in Ref. [18].

IV. EFFECT OF GRID ORIENTATION IN SRD

As pointed out by Ihle *et al.* [15], the underlying cubic grid leads to anisotropy in standard SRD. Concerning the SRD fluid in the bulk, in most practical applications, this anisotropy has only minor influence on the result. In the vicinity of walls, however, the interplay between grid orientation and boundary condition can indeed affect the simulation result. To illustrate this issue, plane Poiseuille flow in a comparatively narrow channel is simulated. The flow is driven by an external acceleration of 5×10^{-2}. All other simulation parameters are equal to those from Sec. II. The channel walls are modeled as bounce-back boundary conditions combined with the commonly used ghost particles proposed in Ref. [18]. The solid line in Fig. 2 represents the velocity profile obtained when the grid is exactly aligned with the channel walls. In contrast, after the grid being rotated by $\pi/4$ with respect to the channel walls, identical simulation parameters lead to the dashed curve. The discrepancy between the two curves demonstrates that, depending on the implemented boundary conditions, the grid orientation can have significant influence on the resulting flow field.

V. ISOTROPIC SRD

A. Description of the method

In standard SRD, even with grid shift, the underlying Cartesian simulation grid induces anisotropy, as shown in the previous section. Using isotropic coarse-graining volumes, this problem can be eliminated in a natural way, and without the necessity of performing random grid rotations [15] to correct for the anisotropy introduced by the lattice. Instead of using cubic lattice cells for coarse graining, we suggest using spheres of constant size, which are randomly distributed over the simulation domain. Consequently, the local mean velocity needed for the collision step [see Eq. (2)] is now evaluated by averaging the velocities of the particles residing in the same sphere, S, that is, $\vec{u}(t)|_i \equiv \langle \vec{v} \rangle^S$, and the thermal velocity of the ith particle is $[\vec{v}_i - \langle \vec{v} \rangle^S]$.

Note that this approach is grid free. For computational efficiency, we use an auxiliary grid to sort the particles into the coarse-graining spheres. This grid is not necessarily Cartesian but can be chosen irregular, such that the union of all grid cells covers the simulation domain. Unlike for standard SRD, this grid does, however, not affect the simulation results, as we will demonstrate in Sec. V F. In analogy to isotropic DSMC [16,17], we refer to this method as *isotropic SRD* (iSRD).

B. Definition of the coarse-graining volumes

In standard SRD with grid shift, the coarse-graining volumes are the cubic cells of a Cartesian grid with a number of basic properties: (i) the coarse-graining volumes are homogeneously distributed in physical space; (ii) the total number of coarse-graining volumes is given by the ratio between domain volume and coarse-graining volume, i.e., it is invariant in time; (iii) at any time, each particle resides in exactly one coarse-graining volume.

We will see that in iSRD these properties do not hold true strictly, but only in a statistical sense. It will be shown, however, that the obtained simulation data agree well with analytical results.

In difference to standard SRD, in iSRD the location of each (spherical) coarse-graining volume is determined randomly. The centers of the coarse-graining spheres shall be uniformly distributed in the simulation domain; however, each unit of physical space contains the same number of coarse-graining spheres only on average. Note that the randomness in the sphere positions has a similar effect as the grid shift in SRD. It reduces precollisional correlations and ensures Galilean invariance.

Sorting the SRD particles into the coarse-graining spheres is a computationally expensive process, as it has to be repeated in each time step. Therefore, we suggest employing an auxiliary grid. In Sec. V F, we will show that this auxiliary grid, while significantly enhancing the efficiency of the simulation, does not affect the simulation result.

The number of coarse-graining spheres, k_l, within cell l of the auxiliary mesh is taken from a Poisson distribution with probability density

$$P_{\Lambda_l}(k_l) = \frac{\Lambda_l^{k_l}}{k_l!} e^{-\Lambda_l} . \tag{11}$$

In the simulation, we first determine the number of coarse-graining spheres in the lth cell according to the distribution P_{Λ_l}, Eq. (11), and then choose the locations of the sphere centers randomly inside the cell. Since particles can be located in more than one coarse-graining volume, they can take part in more than one multiparticle collision per time step. In order to avoid any systematic effect, overlapping coarse-graining spheres should be processed in random order.

The distribution of coarse-graining volumes shall be homogeneous over the domain (i), that is, independent of the cell volume, V_l^C. Therefore, for two arbitrary cells l and l',

$$\frac{\Lambda_l}{\Lambda_{l'}} = \frac{V_l^C}{V_{l'}^C} , \tag{12}$$

that is, the expectation values for the number of coarse-graining volumes in a cell relate as the cell volumes. Together with the normalization condition

$$\sum_l V_l^C = \sum_l \Lambda_l V^S, \tag{13}$$

we obtain

$$\Lambda_l = \frac{V_l^C}{V^S} , \tag{14}$$

where V^S is the volume of a coarse-graining sphere. Summing over all cells and denoting the volume of the entire domain by V, we obtain

$$\Lambda \equiv \sum_l \Lambda_l = \frac{V}{V^S} \tag{15}$$

and, thus, the expectation value for the total number of coarse-graining spheres in a given volume, V, does not depend on the auxiliary grid, that is, (ii) is statistically fulfilled.

Let us finally consider property (iii): The probability that a particle is located in a randomly placed coarse-graining sphere of volume V^S is given by the ratio $V^S/V = 1/\Lambda$, where V is the total volume of the domain. Assume, N coarse-graining spheres are placed randomly and independently

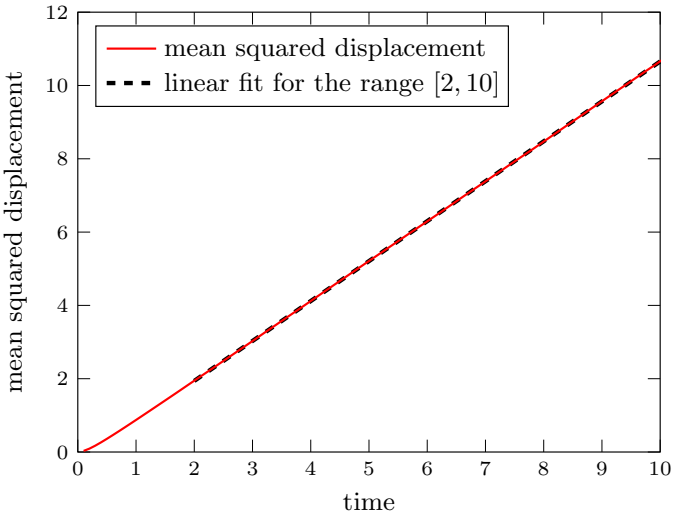

FIG. 3. Mean squared displacement measurement of a force-free system obtained by iSRD. The dashed line shows a linear fit to the simulation data, disregarding the initial transient. The auxiliary grid consists of $32\times32\times32$ cubic cells with side length 1.

in the domain. The probability, A_j, for a certain particle to be simultaneously located in exactly j coarse-graining spheres then obeys a binomial distribution

$$A_j = B(j|N, 1/\Lambda) \approx B(j|\Lambda, 1/\Lambda), \tag{16}$$

where the expectation value for N is given in Eq. (15). Although the total number of coarse-graining spheres is a fluctuating quantity, for the majority of applications the domain volume is much larger than the coarse-graining volume and, therefore, $\Lambda \gg 1$, implying that the relative fluctuations, $\Delta N/N \approx 1/\sqrt{\Lambda}$, are small. We can further exploit the convergence of the binomial distribution to a Poisson distribution, leading to

$$A_j \approx \frac{e^{-1}}{j!}. \tag{17}$$

Thus, the number of coarse-graining spheres, j, a given particle is contained in obeys a Poisson distribution with expectation value 1. Hence, while in standard SRD in each time step each particle is located in exactly one coarse-graining volume, in iSRD this is not the case, and (*iii*) holds true only on average.

C. iSRD for the force-free case: Diffusion

For the first test of the iSRD model, we consider pure diffusion in a periodic domain, being the most simple case. For this simulation and—if not specified otherwise—also for the following simulations we use the diameter of the spherical coarse-graining volume $d = (6/\pi)^{1/3} \approx 1.24$, such that $V^S = 1$. Note that this choice is arbitrary, as d is a free parameter in the model. For our choice, the simulation domain contains on average one coarse-graining sphere per unit volume. Each coarse-graining sphere contains $M = 10$ particles on average. Figure 3 shows the mean squared displacements of the particles. After a short initial transient, the mean squared displacement increases linearly with time. The dashed line shows a linear fit to the simulation data. This indicates that diffusive mass transport is reproduced correctly in iSRD.

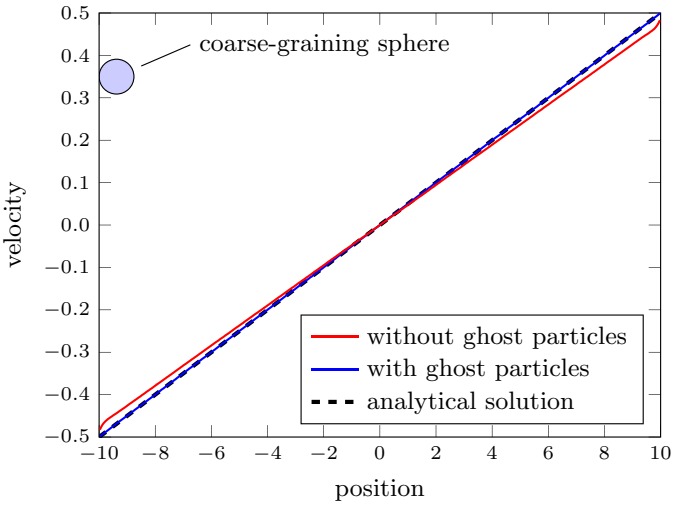

FIG. 4. Couette flow simulated using iSRD with and without ghost particles. The dashed line shows the analytical solution for the given boundary velocities. The size of a coarse-graining sphere is shown at the top left.

D. iSRD for stationary Couette and Poiseuille flow: Momentum transport

To assess the momentum transfer in iSRD, we simulate stationary Couette flow as well as plane Poiseuille flow. In both cases, the walls are modeled through bounce-back boundary conditions [18] once with and once without ghost particles. Further details regarding this aspect are discussed in Sec. V E. Temperature is kept constant by means of the cell-level thermostat described in Refs. [20,21]. Figures 4 and 5 show the velocity profiles obtained from the simulation together with analytical solutions for reference. The viscosity is not known *a priori*, and is therefore determined from the curvature of the flow profiles in Fig. 5.

For both cases, the analytical solution given by the Navier-Stokes equations is recovered, that is, iSRD reproduces the momentum transport correctly, except for the region close to the walls, where we obtain a finite slip, unless ghost particles are employed. The flow profiles obtained from iSRD simulations are smooth and—in contrast to the upper solid line shown in Fig. 1—independent from the underlying spatial discretization. The reason is that the iSRD scheme inherently maintains Galilean invariance.

E. Reducing slip at the walls: Ghost particles

The finite slip at the system walls modeled by simple bounce-back boundaries is a well-known problem of virtually all particle-based, computational fluid dynamics methods; see, for example, Ref. [31]. This behavior, which is undesirable on meso- and macroscopic scales, can be corrected by introducing ghost particles [18,32]. Here, we apply the model developed in Refs. [33,34] for smoothed-particle hydrodynamics (SPH) simulations: In case a coarse-graining sphere reaches out of the domain and into the wall, we mirror the particles from inside the domain at the intersected boundary. The velocity of a ghost particle is computed by inverting the corresponding particle's velocity $\vec{v}_i$ with respect to the wall velocity $\vec{u}_{\text{wall}}$, that is, $\vec{v}_i^{\,\text{ghost}} = 2\,\vec{u}_{\text{wall}} - \vec{v}_i$. In order to make the interaction between fluid and wall symmetric, additional coarse-graining spheres are generated whose centers are located outside the domain. This procedure effectively leads to an extrapolation of the flow velocity beyond the domain boundary.

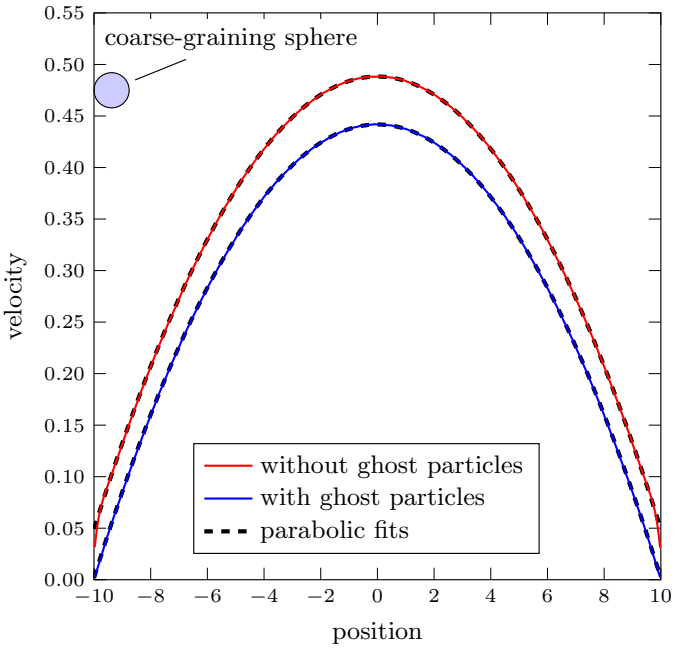

FIG. 5. Plane Poiseuille flow simulated using iSRD with and without ghost particles. The dashed lines are parabolas fitted in the interval $[-5,5]$. For the viscosity, we obtain $\nu = 0.568$ with ghost particles and $\nu = 0.569$ without. In this example, the Reynolds number is approximately 15.5. In dimensional quantities, this would, for example, correspond to water at room temperature (20°C) flowing through a 2-mm-wide channel at velocity 7.8 mm/s.

The blue lines in Figs. 4 and 5 show the flow profiles obtained by iSRD for Couette flow and plane Poiseuille flow where ghost particles are employed. In both cases, we obtain excellent agreement between the simulation results and the theoretical solution.

F. Independence of iSRD on the auxiliary grid

The results of iSRD do not noticeably depend on the chosen auxiliary grid. For demonstration, we compute the velocity profiles for Poiseuille flow in a cubic domain with identical parameters, except for the spatial discretization of the auxiliary grid; see Fig. 6(a). Three cases are investigated: A Cartesian grid [see solid black lines in Fig. 6(b)], a nonuniform regular grid (dashed red lines), and a nonuniform tetrahedral discretization (blue dotted lines). For both considered time step sizes, $\Delta t = 0.1$ and $\Delta t = 1$, the velocity profiles obtained based on the different grids coincide perfectly. Hence, the grid geometry does not affect the simulation results. This is not surprising, since for iSRD the grid is only a data structure intended to accelerate the simulation. This makes iSRD particularly suitable for flows in domains of complex geometric shape, which cannot be meshed uniformly.

VI. TRANSPORT COEFFICIENTS IN ISRD

For standard SRD, Kikuchi *et al.* [28] derive an analytical expression for the kinetic contribution to the viscosity, $\nu_{\mathrm{SRD}}^{\mathrm{kin}}$, by considering the change of velocity correlations $\langle v_x\, v_y \rangle$ in stationary Couette flow due to the action of the streaming and the collision operators. The effect of the streaming operator is the same for SRD and iSRD, while the collision operator acts differently: In SRD at any time, each particle is located in exactly one coarse-graining volume. This is not the case for iSRD. To derive an expression for iSRD which is equivalent to Eq. (7), we consider the effect of

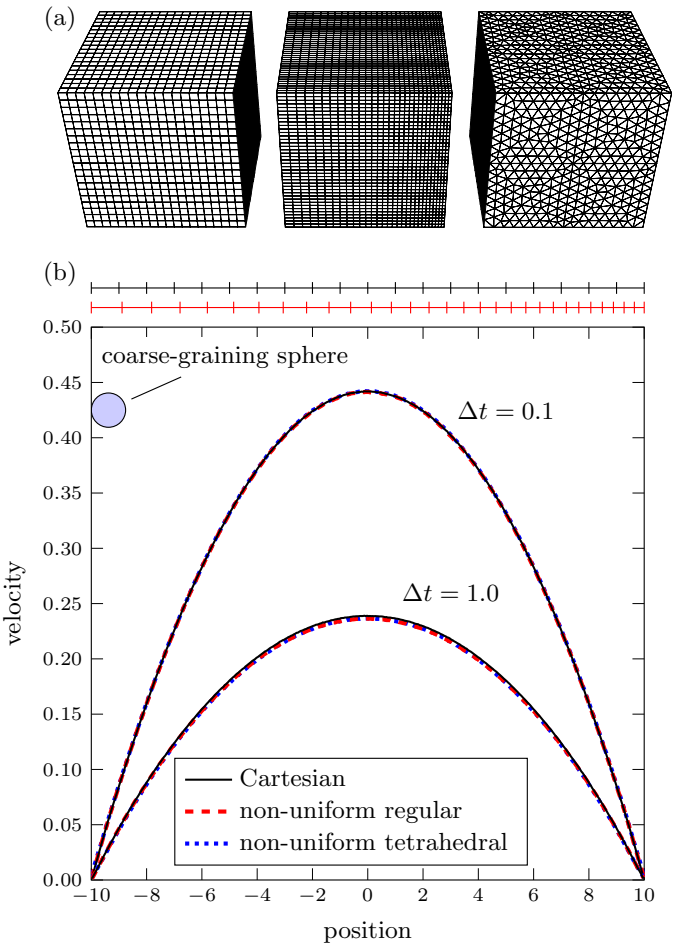

FIG. 6. Plane Poiseuille flow simulated using iSRD, including ghost particles, for the three different auxiliary grids depicted in panel (a). The mesh on the left consists of cubic cells with constant width, as indicated by the black scale in panel (b). The red scale refers to the mesh in the center, comprising nonuniform hexahedra with square basis and varying extent in the direction of the velocity gradient, i.e., normal to the walls. The mesh on the right is composed of nonuniform tetrahedral cells.

the collision operator on the velocity correlation $\langle v_x\, v_y\rangle_i$, referring to particle i under the condition that the particle is contained in $j \in \{0, 1, 2, \dots\}$ coarse-graining spheres. The expectation value of the kinetic contribution to the viscosity, $\nu^{\text{kin}}_{\text{iSRD}}$, is then obtained as a weighted average of these contributions for all j.

If at a certain time step, particle i is not located in any coarse-graining sphere, that is, $j = 0$, the collision step does not change its contribution to the velocity correlation, $\langle v_x\, v_y\rangle_i$. If the particle is contained in exactly one coarse-graining sphere ($j = 1$) the velocity correlation changes according to Eq. (7). For $j = 2$, when the particle is located in two coarse-graining spheres, S_1 and S_2, its contribution to the velocity correlation is

$$\langle v_x(t+\Delta t)v_y(t+\Delta t)\rangle_i = f\left(\alpha, n_{S_1}\right) f\left(\alpha, n_{S_2}\right) \langle v_x(t)v_y(t)\rangle_i, \tag{18}$$

where n_{S_1} and n_{S_2} are the total numbers of particles in these spheres. For the general case, that particle i is contained in exactly j coarse-graining spheres, we have

$$\langle v_x(t+\Delta t)v_y(t+\Delta t)\rangle_i = \langle v_x(t)v_y(t)\rangle_i \prod_{k=1}^{j} f\left(\alpha, n_{S_k}\right) \approx \langle v_x(t)v_y(t)\rangle_i [f(\alpha,M)]^j \,, \tag{19}$$

where we employ Eq. (6) with the approximation that the numbers of particles contained in the coarse-graining volumes are independent. Using the probability, A_j, given in Eq. (17), for finding particle i in j coarse-graining spheres, we define

$$\tilde{f}(\alpha,M) \equiv \sum_j A_j \, f^j(\alpha,M) \overset{\text{Eq. (17)}}{\approx} e^{f(\alpha,M)-1}, \tag{20}$$

and find an expression for the average change of the velocity correlation function due to one collision step in iSRD,

$$\langle v_x(t+\Delta t)\, v_y(t+\Delta t)\rangle = \tilde{f}(\alpha,M)\, \langle v_x(t)\, v_y(t)\rangle, \tag{21}$$

having the same functional form as Eq. (7). Eventually, we obtain the kinetic contribution to the viscosity in iSRD,

$$\nu^{\text{kin}}_{\text{iSRD}} = \frac{k_B\, T}{m} \Delta t \left(\frac{1}{2} + \frac{\tilde{f}}{1-\tilde{f}} \right), \tag{22}$$

which again has the same functional form as $\nu^{\text{kin}}_{\text{SRD}}$, given in Eq. (3). The diffusion coefficient can be derived analogously to the kinetic part of the viscosity. We find

$$D_{\text{iSRD}} = \frac{k_B T}{m} \Delta t \left(\frac{1}{2} + \frac{\tilde{g}}{1-\tilde{g}} \right), \tag{23}$$

with

$$\tilde{g}(\alpha,M) = \sum_j A_j \, g^j(\alpha,M) \overset{\text{Eq. (17)}}{\approx} e^{g(\alpha,M)-1} \,. \tag{24}$$

Note that the shape of the collision bins does not affect the kinetic part of viscosity or the diffusion coefficient. The difference between iSRD and standard SRD comes merely from the fact that the number of collision bins a particle is located in per collision step is distributed differently in iSRD compared to standard SRD. Hence, knowing the size and average number of the coarse-graining volumes is sufficient to compute the kinetic part of viscosity and the diffusion coefficient.

In contrast, for the collisional contribution to viscosity, also the coarse-graining volumes' shape is important. To show this, we follow Ref. [28], and examine the redistribution of momentum due to the collision operator for stationary Couette flow with $\vec{u}(y) = [\dot{\gamma}\, y, 0, 0]$ and constant shear rate $\dot{\gamma} = \partial u_x(y)/\partial y$. We divide the coarse-graining sphere of diameter d into two subvolumes, ① and ②, separated by the plane $\tilde{y} = \tilde{y}_0$ with $0 \leqslant \tilde{y}_0 \leqslant d$, as shown in Fig. 7. The two subvolumes accommodate $n^{(1)}$ and $n^{(2)}$ particles with $n^{(1)} + n^{(2)} = n$, traveling at average velocities $\langle v_x\rangle^{(1)}$ and $\langle v_x\rangle^{(2)}$ in the x direction. The average velocity in the entire coarse-graining sphere is $\langle v_x\rangle^S$. Therefore,

$$\Delta v_x^S \equiv \langle v_x\rangle^{(1)} - \langle v_x\rangle^{(2)} = \frac{n^{(1)} + n^{(2)}}{n^{(2)}} (\langle v_x\rangle^{(1)} - \langle v_x\rangle^S) \,. \tag{25}$$

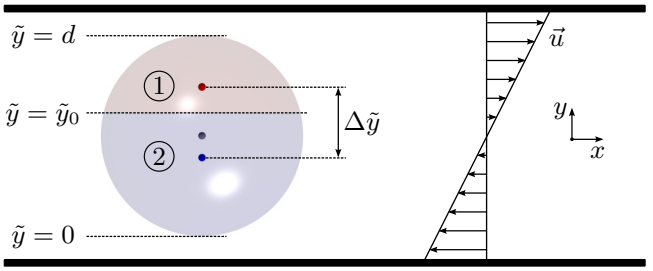

FIG. 7. Redistribution of momentum within one coarse-graining sphere in stationary Couette flow. The coarse-graining sphere is divided into two subvolumes by a horizontal plane at $y = \tilde{y}_0$.

The average distance of pairs of particles picked from different subvolumes, denoted by $\Delta\tilde{y}$, is equal to the distance of the geometric centers of the two subvolumes,

$$\Delta\tilde{y} = \frac{3\,d^3}{8\left(\frac{3}{2}\,d - \tilde{y}_0\right)\left(\tilde{y}_0 - \frac{1}{2}\,d\right)}\,. \tag{26}$$

The collision rule, Eq. (2), conserves momentum. Thus, the transfer of momentum between the subvolumes is equal to the change of momentum in subvolume ① due to the collision step.

The shear stress, σ_{xy}, defined as the transport of momentum per units of time and cross sectional area, is [28]

$$\sigma_{xy} = \frac{m}{A\,\Delta t}\left[\frac{2}{3}n^{(1)}(1-\cos\alpha)\left(\langle v_x\rangle^{(1)} - \langle v_x\rangle^{S}\right)\right], \tag{27}$$

where m is the particle mass and A denotes the characteristic area that the momentum transfer due to one coarse-graining sphere refers to. To obtain A we consider the shaded plane, $A^\star$, in Fig. 8. The average number of spheres intersecting this plane is equal to the expectation value of the number of spheres, $N^\star$, having their centers located in the rectangular cuboid of volume $V^\star \equiv A^\star\,d$,

$$N^\star = \frac{V^\star}{V^S} = \frac{6A^\star}{\pi d^2}\,; \tag{28}$$

thus,

$$A = \frac{A^\star}{N^\star} = \frac{\pi}{6\,d^2}\,. \tag{29}$$

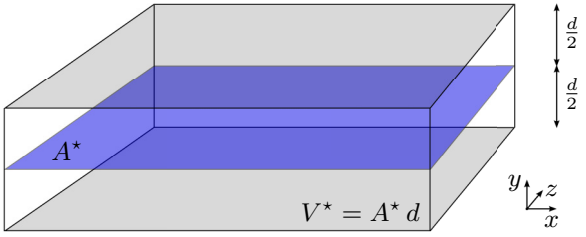

FIG. 8. The characteristic area, A, is the average area that the momentum transport within one single coarse-graining sphere refers to. The size of area A can be obtained considering the average number of coarse-graining spheres, $N^\star$, in a reference volume $V^\star \equiv A^\star\,d$, which is continued periodically in x and z directions.

Combining Eqs. (25) to (27) and (29), and the average mass density in the coarse-graining sphere,

$$\rho = \frac{n\,m}{V^S} = \frac{(n^{(1)} + n^{(2)})\,m}{V^S}\,, \tag{30}$$

we obtain the collisional contribution to viscosity,

$$\nu_{\mathrm{iSRD}}^{\mathrm{coll}} = \frac{\sigma_{xy}}{\rho\,\dot{\gamma}} = \frac{\sigma_{xy}\,\Delta\tilde{y}}{\rho\,\Delta v_x^S} = \frac{n^{(1)}(n-n^{(1)})}{4\,n^2\,\Delta t}\,\frac{d^4(1-\cos\alpha)}{\left(\frac{3}{2}\,d-\tilde{y}_0\right)\left(\tilde{y}_0-\frac{1}{2}\,d\right)}\,. \tag{31}$$

The number of particles $n^{(1)}$ in subvolume ① obeys a binomial distribution, $B(n^{(1)}|n,\,p)$, with probability

$$p = \frac{V^{(1)}}{V^S} = \frac{\tilde{y}_0^2\,(3d-2\tilde{y}_0)}{d^3}\,. \tag{32}$$

Using the property of the binomial distribution,

$$\sum n^{(1)}(n-n^{(1)})\,B(n^{(1)}|n,\,p) = n\,p\,(n-1)\,(1-p)\,, \tag{33}$$

we rewrite Eq. (31) and obtain

$$\nu_{\mathrm{iSRD}}^{\mathrm{coll}} = \frac{(n-1)\,(1-\cos\alpha)}{4n\,\Delta t}\,\frac{2d\,\tilde{y}_0^2}{\tilde{y}_0+\frac{1}{2}d}\left[1-\frac{\tilde{y}_0^2\,(3d-2\tilde{y}_0)}{d^3}\right]. \tag{34}$$

Averaging over the position of the plane with respect to the coarse-graining sphere, $\tilde{y}_0$, which is uniformly distributed in $[0,\,d]$, yields

$$\nu_{\mathrm{iSRD}}^{\mathrm{coll}} = \frac{(n-1)\,(1-\cos\alpha)}{4\,n\,\Delta t}\,\frac{2\,d^2}{15} \tag{35}$$

and averaging over n, which is, in good approximation, Poisson distributed, leads to the final expression for the collisional contribution to the viscosity coefficient in iSRD,

$$\nu_{\mathrm{iSRD}}^{\mathrm{coll}} = \frac{d^2}{30\Delta t}\,\frac{M-1+e^{-M}}{M}(1-\cos\alpha). \tag{36}$$

Note that Eq. (36) has the same functional form as the corresponding expression for standard SRD, $\nu_{\mathrm{SRD}}^{\mathrm{coll}}$, given by Eq. (10).

VII. QUANTITATIVE VALIDATION OF ISRD

A. Benchmarking cases

To check the validity of the analytical expressions for the diffusion coefficient and the kinematic viscosity given by Eqs. (22), (23), and (36) we compare them to corresponding iSRD simulation results. We consider two physical systems, force-free fluid and plane Poiseuille flow. The parameters we vary, are the time step Δt, the rotation angle α, and the average number of particles per coarse-graining sphere M. The other parameters are kept constant. We treat time and position as dimensionless parameters. Thus, the viscosity and the diffusion coefficient are considered in dimensionless form, as well.

B. Diffusion coefficient

The diffusion coefficient is computed from the mean squared displacement of the particles in a cubic domain with side length 16. The simulation domain is periodically continued in all directions, and no external force acts on the particles. The numerical result is averaged over several individual measurements for each parameter set to reduce statistical errors. Two different time steps, $\Delta t = 0.1$ and $\Delta t = 1$, are considered. Figure 9 shows the diffusion coefficient in dependence on the rotation angle,

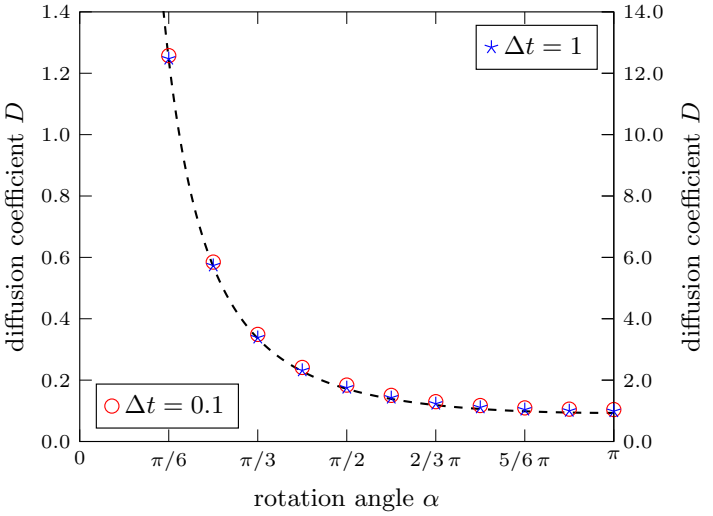

FIG. 9. Diffusion coefficient as a function of the rotation angle, α, for two different time steps and $M = 10$ particles per coarse-graining sphere on average. The left and right vertical axes refer to the data for $\Delta t = 0.1$ and $\Delta t = 1$, respectively. The dashed line shows the theoretical result, Eq. (23).

α. The theoretical result, given by Eq. (23), is indicated by the dashed line. The simulation data (symbols in Fig. 9) are in excellent agreement with the theoretical results over the full range of the rotation angle.

The numerical simulation results for the diffusion coefficient as a function of the average number of particles per coarse-graining sphere are shown in Fig. 10. For large number of particles, M, the theoretical result, Eq. (23), is well reproduced for both considered time steps, $\Delta t = 0.1$ and $\Delta t = 1$, indicated by the good agreement of the numerical data (symbols in Fig. 10) with the dashed line

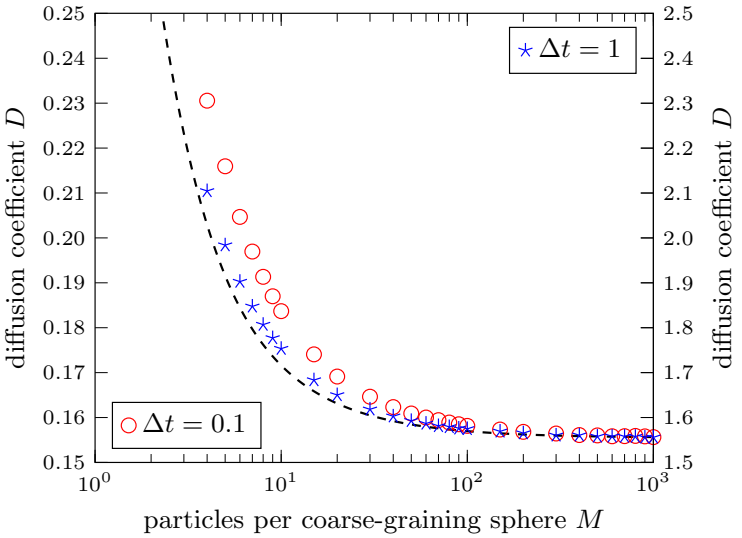

FIG. 10. Diffusion coefficient as a function of the average number of particles per coarse-graining sphere, M, for two different time steps and $\alpha = \pi/2$. The left and right vertical axes refer to the data for $\Delta t = 0.1$ and $\Delta t = 1$, respectively. The dashed line shows the theoretical result, Eq. (23).

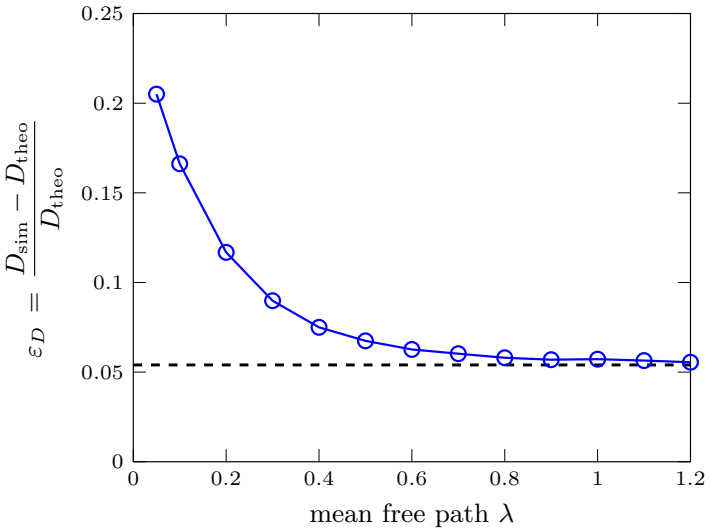

FIG. 11. Relative deviation between the diffusion coefficient measured in simulations, D_{sim}, and the analytical result from Eq. (23), denoted as D_{theo}, over the mean free path, λ, which is equal to the time step for the chosen parameters. To yield a pronounced correlation contribution, α and M are chosen as 130° and 5, respectively [35].

showing the diffusion coefficient, as given by Eq. (23). For smaller M, however, the simulation data deviate from the analytical results. One source for this deviation is the assumption that the number of particles within overlapping coarse-graining spheres is independent, which was exploited in the derivation of the transport coefficients. For large M, the relative fluctuations in particle number are small, rendering this effect negligible. At least for the smaller time step, $\Delta t = 0.1$, another influence is relevant. It is known for standard SRD, that at low particle density and small mean free path there are significant correlation contributions to the kinetic part of viscosity and diffusion coefficient. For the viscosity, this effect is masked by the collisional contribution, which is dominant in this regime. For the diffusion coefficient, which has no collisional contribution, the impact is significant [24,35], which agrees with the results shown in Fig. 10.

For comparison with Ref. [35], the relative deviation between measured and predicted diffusion coefficient, ε_D, is depicted in Fig. 11 depending on the mean free path for $M = 5$ and $\alpha = 130°$. As the mean free path, λ, is increased, for the considered parameters, ε_D does not approach zero but approximately 5.4%, indicated by the dashed horizontal line. One may therefore divide ε_D into two parts. The first one vanishes with increasing λ, and is attributed to correlations similar to those discussed in previous works [24,35]. In contrast, the second part does not depend on the mean free path. The source for the second part is that particle numbers in overlapping spheres are correlated and that in the iSRD scheme a given particle may interact with other particles more than once per collision step. As Fig. 10 indicates, both the first part and the second part of ε_D approach zero as M is increased. Moreover, comparing the results depicted in Fig. 11 to those of Ref. [35] shows that for small λ, randomly distributed spheres reduce correlations more effectively than the grid shift. In Ref. [35], the exponential term from Eq. (9) is neglected when computing the theoretical prediction for the diffusion coefficient, while in this study it is considered. Neglecting this term here does not change Fig. 11 noticeably.

C. Kinematic viscosity

We determine the kinematic viscosity from the velocity profile's curvature for plane Poiseuille flow in the steady state. The simulation domain is cubic with side length 20. The number of

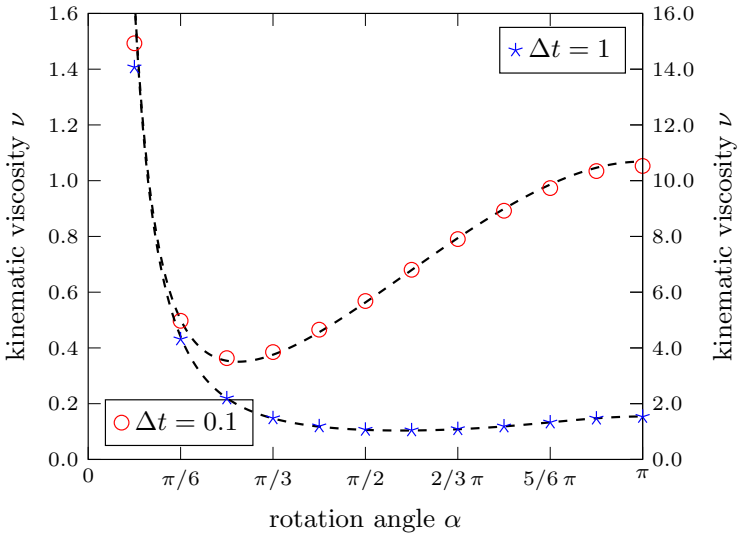

FIG. 12. Kinematic viscosity as a function of the rotation angle, α, for two different time steps and $M = 10$ particles per coarse-graining sphere on average. The left and right vertical axes refer to the data for $\Delta t = 0.1$ and $\Delta t = 1$, respectively. The dashed line shows the theoretical result, Eqs. (22) and (36).

simulated time steps, N_t, is chosen such that $N_t\, M = 16{\times}10^6$, resulting in smooth profiles and small fluctuations of the viscosity. The mean free path and, thus, the transport coefficients depend sensitively on temperature. Therefore, we maintain a constant temperature by means of the cell-level thermostat described in Refs. [20,21]. Figure 12 shows the simulation results for both $\Delta t = 0.1$, where the collisional contribution to viscosity dominates, and $\Delta t = 1$, where the kinetic contribution dominates. The simulation data for the viscosity as a function of the rotation angle show excellent agreement with the analytical results, Eqs. (22) and (36). For the small time step, $\Delta t = 0.1$, we obtain minor deviations, which are even less distinct for $\Delta t = 1$. Figure 13 shows the viscosity as a function of the average number of particles per coarse-graining volume, M. We obtain minor, systematic deviations for both values of Δt, which we attribute to the thermostat, since such deviations are not apparent in the diffusion coefficient, where no thermostat is used. For the considered time steps, $\Delta t = 0.1$ and $\Delta t = 1$, the simulation results for large M deviate from the theoretical results [Eqs. (22) and (36)] by approximately 0.3% and 0.5%, respectively. Similar to the diffusion coefficient discussed above, we also perceive systematic deviations between the simulation data and the theoretical results at small particle number. For the viscosity, this error is less pronounced than in case of the diffusion coefficient, which again matches previous findings [24,35].

VIII. PERFORMANCE STUDY

To give an idea about the computational performance of iSRD, we compare it to traditional SRD, simulating fluid at rest within a cubic domain with side length 20 and periodic boundaries in all directions. Both implementations are based on an existing simulation framework [19].

In our SRD implementation, each time step comprises the following substeps: First, the particles are propagated according to their current velocity (*streaming step*). In this step, also the periodic boundary is imposed. Second, the particles are sorted into the shifted grid in order to compute the cell-averaged velocities, which are needed to perform the multiparticle collision. Third, the relative particle velocities are rotated (*collision step*). Finally, a cell-level thermostat [20,21] is applied to the nonshifted grid keeping the average temperature constant. The cell width is $a = 1$, and the simulation grid is aligned with the cubic domain.

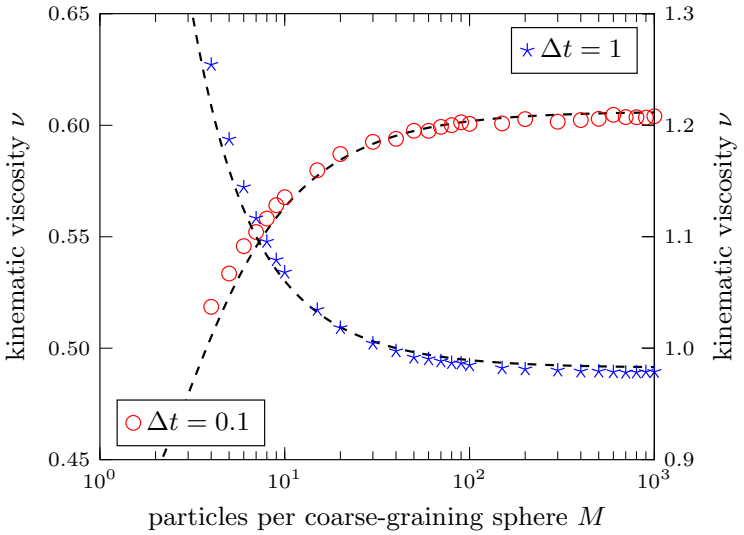

FIG. 13. Kinematic viscosity as a function of the average number of particles per coarse-graining sphere, M, for two different time steps and $\alpha = \pi/2$. The left and right vertical axes refer to the data for $\Delta t = 0.1$ and $\Delta t = 1$, respectively. The line shows the theoretical result, Eqs. (22) and (36).

The procedure for the iSRD simulations is very similar. However, the second and third steps are replaced by the algorithm described in Secs. V A and V B. As auxiliary grid and also for the thermostat, the nonshifted grid from the SRD simulations is used. For a fair comparison, the volume and number of collision bins should be equal. The coarse-graining sphere diameter is, therefore, chosen as $d = (6/\pi)^{1/3} \approx 1.24$, resulting in $V^S = 1$.

On average, $M = 10$ particles are in each collision volume. We choose the time step and the rotation angle as $\Delta t = 0.1$ and $\alpha = \pi/2$, respectively. Each simulation runs for 10^4 time steps on an Intel Core i7-4790K processor. When restricted to one single thread, we find iSRD to be approximately twice as time-consuming as standard SRD. Increasing the number of threads, SRD and iSRD scale similarly.

IX. CONCLUSION

We have introduced isotropic SRD, which is a modification of standard SRD. Instead of using Cartesian grid cells as coarse-graining volumes, we generate coarse-graining spheres randomly within the simulation domain. This allows to maintain Galilean invariance without the need for a grid shift. The proposed particle-based fluid simulation method is isotropic by construction and truly grid free. Merely an auxiliary grid is needed in order to efficiently sort the particles into the coarse-graining spheres. While the structure of the auxiliary grid can affect the computational cost, we demonstrate that it does not affect the simulation results. The proposed algorithm is, therefore, particularly suitable to simulate the fluid flow through domains of complicated shape.

Moreover, we show that iSRD reproduces both mass and momentum transport correctly. We also provide analytical expressions for the transport coefficients depending on the simulation parameters. The measured values for the transport coefficients accurately follow these expressions, especially for higher particle numbers per coarse-graining volume. Further, the use of spheres as coarse-graining volumes prevents the existence of preferred directions for momentum transport, yielding a fully isotropic simulation method, even for situations with large gradients.

For both iSRD and SRD, the mean free path does not depend on the density, and therefore, the known dependence of the transport coefficients in gases on density and temperature is not recovered.

Introducing an additional temperature-dependent collision probability, as proposed by Gompper *et al.* [1], allows the time step Δt to be controlled locally. Since the diffusion coefficient is proportional to Δt, this idea renders the diffusion coefficient freely adjustable. Viscosity, however, cannot be adjusted similarly, because it has one component proportional to Δt and another one proportional to $1/\Delta t$. In iSRD, the diameter of the coarse-graining spheres is, in principle, locally adjustable, as well. Exploiting this should allow the correct dependence for the viscosity to be recovered. The concrete implementation is, however, not straightforward, since changing the diameter also changes the average particle number per coarse-graining volume. For the relations introduced in Sec. VI to hold, the number density of coarse-graining spheres has to be adjusted accordingly, so that each particle is on average contained in one coarse-graining volume per collision step. In addition to time step and diameter, one can also adjust the rotation angle locally, yielding three control parameters in total. Following this approach, iSRD is expected to be able to simultaneously reproduce not only the correct density and temperature dependence for the diffusion coefficient and the viscosity, but also for the heat conductivity.

ACKNOWLEDGMENTS

We thank Dan Serero for sharing his expertise in kinetic theory and Kuang-Wu Lee for fruitful discussions regarding stochastic rotation dynamics. We also thank the Deutsche Forschungsgemeinschaft (DFG) for funding through the Cluster of Excellence "Engineering of Advanced Materials," ZISC, and FPS.

[1] G. Gompper, T. Ihle, D. M. Kroll, and R. G. Winkler, Multi-particle collision dynamics: A particle-based mesoscale simulation approach to the hydrodynamics of complex fluids, in *Advanced Computer Simulation Approaches for Soft Matter Sciences III*, edited by C. Holm and K. Kremer, Advances in Polymer Science Vol. 221 (Springer, Berlin, 2009), pp. 1–87.

[2] M. Ripoll, R. G. Winkler, K. Mussawisade, and G. Gompper, Mesoscale hydrodynamics simulations of attractive rod-like colloids in shear flow, J. Phys.: Condens. Matter **20**, 404209 (2008).

[3] M. Yang and M. Ripoll, Thermophoretically induced flow field around a colloidal particle, Soft Matter **9**, 4661 (2013).

[4] E. Tüzel, G. Pan, T. Ihle, and D. M. Kroll, Mesoscopic model for the fluctuating hydrodynamics of binary and ternary mixtures, Europhys. Lett. **80**, 40010 (2007).

[5] E. Tüzel, G. Pan, and D. M. Kroll, Dynamics of thermally driven capillary waves for two-dimensional droplets, J. Chem. Phys. **132**, 174701 (2010).

[6] J. M. Haile, *Molecular Dynamics Simulation: Elementary Methods* (Wiley, New York, 1997).

[7] G. A. Bird, *Molecular Gas Dynamics and the Direct Simulation of Gas Flows*, Molecular Gas Dynamics and the Direct Simulation of Gas Flows Vol. 1 (Clarendon Press, New York, 1994).

[8] J. J. Brey, D. Cubero, F. Moreno, and M. J. Ruiz-Montero, Fourier state of a fluidized granular gas, Europhys. Lett. **53**, 432 (2001).

[9] G. A. Bird, The velocity distribution function within a shock wave, J. Fluid Mech. **30**, 479 (1967).

[10] G. A. Bird, Perception of numerical methods in rarefied gasdynamics, in *Proceedings of the 16th International Symposium on Rarefied Gas Dynamics: Theoretical and Computational Techniques*, ser. Progress in Astronautics and Aeronautics (American Institute of Aeronautics and Astronautics, Reston, VA, 1989), pp. 211–226.

[11] C. Cercignani, *The Boltzmann Equation and Its Applications*, Applied Mathematical Sciences Vol. 67 (Springer, New York, 1988).

[12] G. E. Karniadakis, A. Beskok, and N. Aluru, *Microflows and Nanoflows: Fundamentals and Simulation*, edited by S. S. Antman, L. Greengard, and P. J. Holmes, Interdisciplinary Applied Mathematics No. 29 (Springer, New York, 2005).

[13] A. Malevanets and R. Kapral, Mesoscopic model for solvent dynamics, J. Chem. Phys. **110**, 8605 (1999).
[14] T. Ihle and D. M. Kroll, Stochastic rotation dynamics: A Galilean-invariant mesoscopic model for fluid flow, Phys. Rev. E **63**, 020201 (2001).
[15] T. Ihle and D. M. Kroll, Stochastic rotation dynamics, I: Formalism, Galilean invariance, and Green-Kubo relations, Phys. Rev. E **67**, 066705 (2003).
[16] A. Donev, B. J. Alder, and A. L. Garcia, Stochastic Hard-Sphere Dynamics for Hydrodynamics of Nonideal Fluids, Phys. Rev. Lett. **101**, 075902 (2008).
[17] A. Donev, B. J. Alder, and A. L. Garcia, A thermodynamically consistent non-ideal stochastic hard-sphere fluid, J. Stat. Mech. (2009) P11008.
[18] A. Lamura, G. Gompper, T. Ihle, and D. M. Kroll, Multi-particle collision dynamics: Flow around a circular and a square cylinder, Europhys. Lett. **56**, 319 (2001).
[19] S. Strobl, Mesoscopic particle-based fluid dynamics in complex geometries, Ph.D. thesis, Friedrich-Alexander-Universität Erlangen-Nürnberg, Erlangen, 2017.
[20] M. Hecht, J. Harting, T. Ihle, and H. J. Herrmann, Simulation of claylike colloids, Phys. Rev. E **72**, 011408 (2005).
[21] M. Hecht, Simulation of peloids, Ph.D. thesis, Universität Stuttgart, Stuttgart, Germany, 2007, http://dx.doi.org/10.18419/opus-4795.
[22] D. M. Heyes, Molecular dynamics at constant pressure and temperature, Chem. Phys. **82**, 285 (1983).
[23] M. P. Allen and D. J. Tildesley, *Computer Simulation of Liquids* (Clarendon Press, New York, 1989).
[24] E. Tüzel, T. Ihle, and D. M. Kroll, Dynamic correlations in stochastic rotation dynamics, Phys. Rev. E **74**, 056702 (2006).
[25] T. Ihle and D. M. Kroll, Stochastic rotation dynamics. II. Transport coefficients, numerics, and long-time tails, Phys. Rev. E **67**, 066706 (2003).
[26] T. Ihle, E. Tüzel, and D. M. Kroll, Equilibrium calculation of transport coefficients for a fluid-particle model, Phys. Rev. E **72**, 046707 (2005).
[27] T. Ihle, Chapman-Enskog expansion for multi-particle collision models, Phys. Chem. Chem. Phys. **11**, 9667 (2009).
[28] N. Kikuchi, C. M. Pooley, J. F. Ryder, and J. M. Yeomans, Transport coefficients of a mesoscopic fluid dynamics model, J. Chem. Phys. **119**, 6388 (2003).
[29] C. M. Pooley and J. M. Yeomans, Kinetic theory derivation of the transport coefficients of stochastic rotation dynamics, J. Phys. Chem. B **109**, 6505 (2005).
[30] T. Ihle, E. Tüzel, and D. M. Kroll, Resummed Green-Kubo relations for a fluctuating fluid-particle model, Phys. Rev. E **70**, 035701 (2004).
[31] I. V. Pivkin and G. E. Karniadakis, A new method to impose no-slip boundary conditions in dissipative particle dynamics, J. Comput. Phys. **207**, 114 (2005).
[32] D. S. Bolintineanu, J. B. Lechman, S. J. Plimpton, and G. S. Grest, No-slip boundary conditions and forced flow in multiparticle collision dynamics, Phys. Rev. E **86**, 066703 (2012).
[33] S. J. Cummins and M. Rudman, An SPH projection method, J. Comput. Phys. **152**, 584 (1999).
[34] K. Szewc, J. Pozorski, and J.-P. Minier, Analysis of the incompressibility constraint in the smoothed particle hydrodynamics method, Int. J. Num. Meth. Eng. **92**, 343 (2012).
[35] M. Ripoll, K. Mussawisade, R. G. Winkler, and G. Gompper, Dynamic regimes of fluids simulated by multiparticle-collision dynamics, Phys. Rev. E **72**, 016701 (2005).